Size-dependent local conductance properties of CdSe nanocrystal ensembles

D. Toker,[1] I. Balberg,[1,*] O. Zelaya-Angel,[2] E. Savir,[1] and O. Millo[1,†]

[1]*Racah Institute of Physics and the Center for Nanoscience and Nanotechnology, The Hebrew University of Jerusalem, Jerusalem 91904, Israel*

[2]*Departemento de Fisica, Centro de Investigacion de Estudios Avanzados, P. O. Box, 14-740, Mexico City 07360 Distrito Federal, Mexico*

(Received 26 July 2005; published 19 January 2006)

Applying conductance atomic force microscopy to measure the local current routes in ensembles of CdSe nanocrystallites of diameters in the range of 8–12 nm, we found that the electrical transport takes place through the crystallites themselves rather than along their grain boundaries. Statistical analysis of the current images, in correlation with macroscopic electrical transport measurements, reveals a crossover between two different conduction regimes. The behavior in each regime is found to be governed by the average diameter of the nanocrystals in the ensemble. We interpret the above findings as a transport manifestation of the quantum confinement effect.

DOI: 10.1103/PhysRevB.73.045317 PACS number(s): 73.63.Bd, 72.20.−i, 68.37.Ps

INTRODUCTION

Semiconductor nanocrystals (NCs), also known as quantum dots or artificial atoms, have attracted much interest in recent years[1,2] as they mark the transition between the atomic or molecular and the bulk solid-state regimes. These particles contain hundreds to thousands of atoms and retain a crystalline structure with the periodicity of the bulk semiconductor. Yet the wave functions of charge carriers in them are confined to the small dimensions of the NC, and thus they have a discrete energy level structure, reminiscent of single atoms. A step toward understanding the emergence of the macroscopic behavior in NCs is in the study of materials consisting of ensembles of such particles (in addition to monitoring the evolution of the single-particle electronic level structure with the size of the NCs). The transition from isolated NCs, the "artificial atoms," to "quantum-dot solids" in CdSe has already been found to manifest itself in the modification of the optical properties such as a redshift of the excitonic band gap, with respect to the individual NCs, as a function of the average size of the individual crystallites.[3–5] These observations were accounted for by the formation of extended electronic states resulting from the overlap between the electronic wave functions of neighboring NCs, in analogy to the interaction between atoms in bulk solids.

While progress has been made in the understanding of the optical properties and the electronic structure of NC ensembles, the electrical conductance properties in such systems are understood only at a rudimentary level. In particular, while electrical transport through individual semiconductor NCs has been extensively investigated[6–12] [mainly by employing scanning tunneling microscopy (STM), conductive atomic force microscopy (CAFM), and tunnel junctions prepared by nanolithography], the transport properties of semiconductor NC solids[12–14] have not yet been locally investigated. This in contrast with the advancement that has been made in the understanding of the local transport properties of various conductive nanoparticle ensembles such as granular metals[15,16] and ensembles of microparticles such as carbon black–Polymer systems[16–18] and microcrystalline semiconductors.[19–21]

In our recent application of C-AFM for the determination of the local conductivity of the above systems and the correlations we found with "macroscopic" observations, we have shown that such studies shed light on the conduction mechanism as well as resolve other fundamental issues: monitoring of the current routes in hydrogenated microcrystalline silicon (μc-Si:H),[20] the interplay between percolation and tunneling in metal-insulator composites,[15–18] and the electrothermal switching effect in carbon black-polymer composites.[16,18] Following those advancements, we report here the application of C-AFM and STM for the local study of the electical transport in large (macroscopic) ensembles of CdSe nanocrystals, noting that the latter is a model system of a quantum-dot solid. We show that, in contrast to the case of μc-Si:H, where the current was found to flow predominantly along the silicon disordered tissue that encapsulates the crystallite aggregates or the individual crystallites,[20] the current in the CdSe assemblies flows through the nanocrystallites. In addition, the local C-AFM data, when correlated with the global transport measurements, reveal significantly different transport behaviors for samples consisting of NCs with an average diameter smaller than ~10 nm compared to those that are formed of NCs with average diameters larger than 11 nm. The fact that the excitonic Bohr radius of CdSe is[2] ~5.6 nm suggests that the differences mentioned above are associated with the quantum confinement effect.

EXPERIMENT

The nanocrystalline CdSe films, 200 nm thick, were grown on glass substrates by the chemical bath deposition method at different deposition temperatures (T_d).[3] The resulting samples contain several layers of NCs. The average crystallite diameter (D) was found to increase monotonically in the range of our deposition temperatures (0 to 80 °C) from about 8 to about 13 nm, and the size distribution (for each sample) is typically ~20%. We have estimated the size of our NCs in the present study from transmission electron microscopy (TEM) and scanning electron microscopy (SEM) as

well as from our STM images such as the ones shown below. The dominant crystalline structure of the NCs (that was determined by x-ray and electron diffraction measurements) was found to change from hexagonal wurtzite for T_d up to $\sim 30\ ^\circ\mathrm{C}$ (where $D<10$ nm) to zinc blende at T_d above $\sim 50\ ^\circ\mathrm{C}$ (where $D>11$ nm). It must be noted, however, that in each sample some contribution of the second (minority) phase was found, while the transition region ($T_d \sim 40\ ^\circ\mathrm{C}$) shows a substantial amount of both phases.

Previous studies[3] of the optical absorption of the films containing the above NCs have exhibited a clear quantum confinement effect for the smaller-D (and composed mostly of wurtzite NCs) systems, which is manifested by the widening of the optical band gap with decreasing D. Correspondingly, as will be shown below, there is a (macroscopic) conductivity jump of seven orders of magnitude between samples of T_d lower than 15 °C and samples of $T_d>50\ ^\circ\mathrm{C}$. In this work we focus mainly on the samples of $T_d=15\ ^\circ\mathrm{C}$, for which $D<10$ nm (hereafter the small NC), $T_d=40\ ^\circ\mathrm{C}$, for which $D\sim 10.5$ nm, and $T_d=60\ ^\circ\mathrm{C}$, for which $D>11$ nm (hereafter the large NC). Each of these represents one of the above regimes.

The CAFM measurements were performed at room temperature with a commercial scanning force microscope (NT-MDT Solver) in the constant-force mode, where current maps were obtained along with the topography.[17] The current was measured between the AFM conductive tip and a counterelectrode deposited on one side of the film, for a constant tip-sample bias voltage. The AFM tip typically scanned the sample at distances of a few millimeters from the counterelectrode. Thus, current was detected only when there was a macroscopic conducting path between the tip and the electrode. We have used Ti-Pt-coated (conductive) tips having a curvature of ~50 nm, which is larger than the NC diameters. Consequently, the topographic images are not expected to resolve the individual NCs. Indeed, the images obtained exhibit grains of up to 20 nm in height, having an average lateral diameter of about 100 nm, which we attribute to NC aggregates. This was confirmed by STM measurements (performed on the most conducting samples, see below) that could resolve both the individual NCs and their aggregates. Figure 1 portrays STM (a) and (b) and AFM (c) topographic images acquired at two different locations on a sample of large NCs. The STM images clearly show that the large grains observed in the AFM map are in effect composed of many smaller particles, corresponding to the individual NCs. Figure 1(d) presents the current image corresponding to Fig. 1(c) that was acquired with a sample bias of $V_B=-1$ V, showing a spatial resolution superior to that of the AFM topography. This allows us to discriminate between different current intensities along an aggregate. We show below that a statistical analysis of such current maps in correlation with the topography provides a means for comparison between the different behaviors of the above three types of samples.

RESULTS

In Fig. 2 we plot the macroscopic conductivity as a function of temperature for representative samples of different deposition temperatures (T_d) and mostly wurtzite structure) the temperature dependence of the conductivity is significantly stronger than that for samples in the large-NC-diameter regime ($T_d \geqslant 50\ ^\circ\mathrm{C}$). The conductivity of the former appears to be simply activated (in the limited temperature range available) with an activation energy of a few tenths of an eV, increasing with decrease of the NC size. The conductivity improves

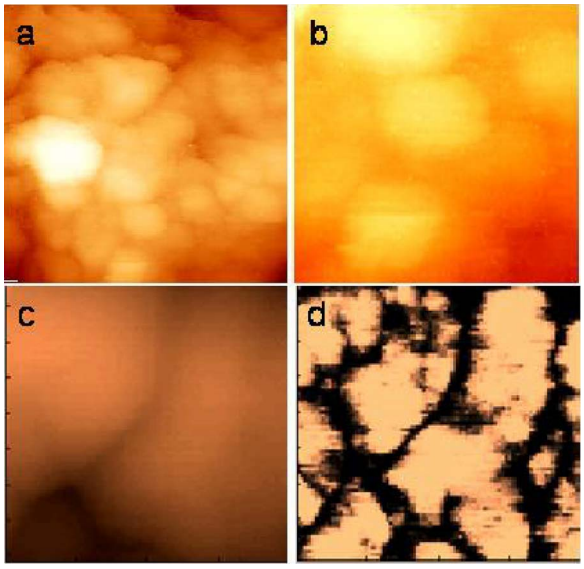

FIG. 1. (Color online) 80×80 (a) and 30×30 (b) nm^2 STM topographic images measured on a sample with an ensemble of large NCs. A CAFM topography measurement (80×80 nm^2) performed on the same sample but at a different location is presented in (c) and the simultaneously measured current map (at $V_B=-1$ V) in (d). The topographic height range is 30 nm and the current range is 0–20 nA.

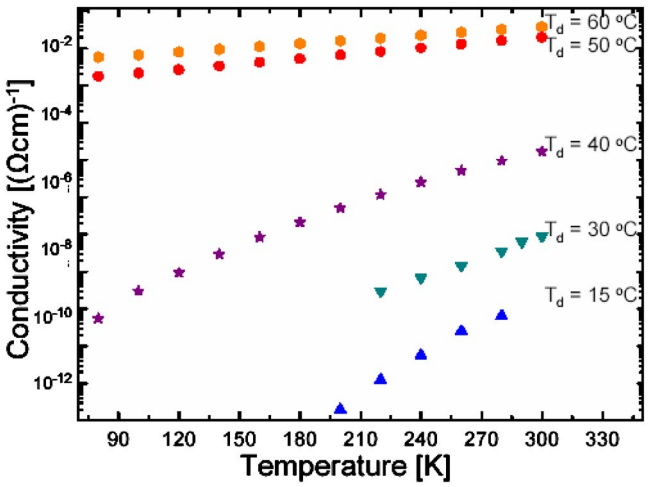

FIG. 2. (Color online) Conductivity as a function of temperature for samples of different deposition temperatures T_d, as marked in the figure. The average NC diameter of these samples increases monotonically and is less than 10 nm for the samples of $T_d<30\ ^\circ\mathrm{C}$, about 10.5 for the samples of $T_d\sim 40\ ^\circ\mathrm{C}$, and larger than 11 nm for $T_d>50\ ^\circ\mathrm{C}$.

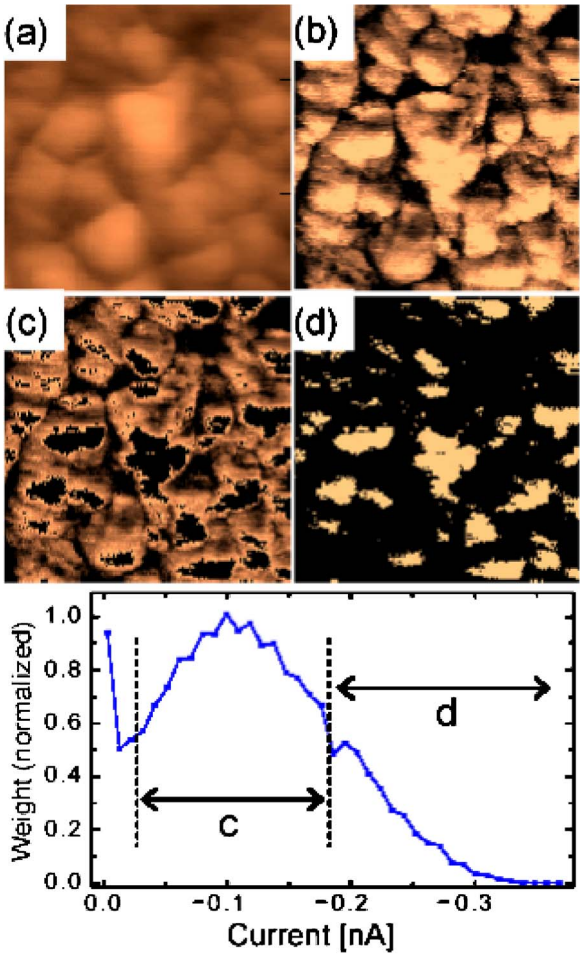

FIG. 3. (Color online) 500×500 nm^2 topography (a) and corresponding current map at $V_B=-4.75$ V (b) obtained on a sample of small NCs. (c) and (d) portray partial current images corresponding to the current ranges marked in the histogram presented in (e).

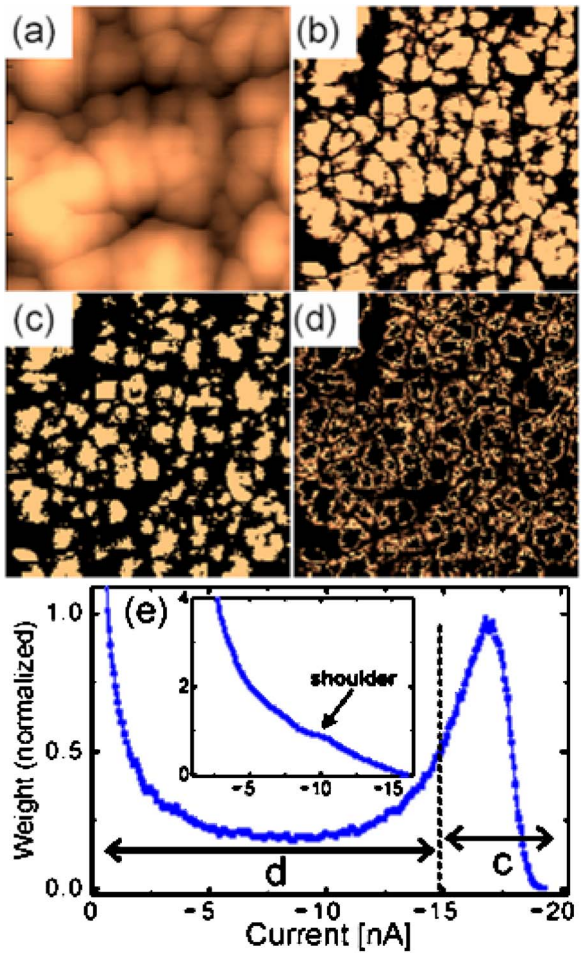

FIG. 4. (Color online) 500×500 nm^2 topography (a) and corresponding current map at $V_B=-1$ V (b) obtained on a sample of large NCs. (c) and (d) portray partial current images corresponding to the current ranges marked in the histogram presented in (e). The inset of (e) presents the histogram of a current map acquired at $V_B=-0.5$ V, which is below V_{th}.

substantially for the intermediate (mixed phase) sample of $D\sim10.5$ nm ($T_d=40$ °C), but is still several orders of magnitude lower than that of the samples with NC diameters larger than 11 nm ($T_d>50$ °C and composed mostly of zinc-blende NCs), where for the latter (considering the fact that the Bohr radius in CdSe is[2] ~5.6 nm) strong confinement is not expected to hold. In order to learn more about the conduction mechanism, we turned to local probing of the conductance properties using the CAFM technique.

In Figs. 3 and 4 the simultaneously measured AFM topography (a) and current maps (b) are shown for the samples of the large and small NCs, respectively. The currents correlate well with the topography and they are present on top of the aggregates rather than around them. For a high enough bias, a measurable current (well above the noise level) is detected all over the area corresponding to the aggregates, with its intensity decreasing toward their edges. The lowest currents in each scan are always found between the aggregates. It is therefore reasonable to conclude that the current between the AFM tip and the counterelectrode flows through the NCs and not along the aggregate edges. This is in contrast to our previous findings on polycrystalline CdS (Ref. 19) and μc-Si:H,[20] where the current was found to flow along the edges of the crystallites or the crystallite aggregates. Figures 3(c), 3(d), 4(c), and 4(d) are the "partial current maps" to be discussed below.

In order to study the statistics of the current distribution, histograms were taken from the current maps. Figures 3(e) and 4(e) show the histograms corresponding to Figs. 3(b) and 4(b), respectively. The peak observed in these histograms appears for other samples as well, whenever the bias voltage exceeds a certain threshold V_{th}. For the samples of small NC diameter the peak is always located at the lower current region, whereas for the samples of large NCs the peak is shifted toward the higher end of the current range. It is important to note here the conditions needed for the emergence of the peaks in the histograms and the way they are affected. The current histograms of the small NC samples at low bias voltages are similar to those at higher bias voltages, but with the peak not fully developed and hardly discernible from the measurement noise (~20 pA). The evolution of the current peak for the large-NC sample is quite different. Here, at low bias voltages the histograms exhibit a "shoulder" at the larger current range [see inset to Fig. 4(e)], which is

actually a precursor that heralds the emergence of a new peak. Thus, each sample can be characterized by two thresholds, one for the detection of current above the noise level and the other for the formation of a peak in the current histogram (V_{th}). These thresholds as well as the maximal current measured in each scan provide a means for the comparison of the conductivity of different samples. The conductivity, according to these criteria, increases monotonically with the average diameter of the NCs, consistent with the macroscopic transport data (Fig. 2).

The current map of Fig. 3(b), for the small-NC sample, is decomposed in Figs. 3(c) and 3(d) into partial current maps in which only the currents pertaining to a specific range are drawn. Specifically, Fig. 3(c) shows only the currents corresponding to the histogram peak, as marked in Fig. 3(e), whereas Fig. 3(d) shows the higher-current region [region *d* in Fig. 3(e)]. It is evident that while the peak currents cover most of the aggregate area [Fig. 3(c)], there is a significant contribution of higher-current enclosures [Fig. 3(d)]. These enclosures may be a signature of preferred current routes starting from specific NCs within an aggregate. Figure 4 presents an analogous partial current map analysis for the sample of the large NCs. Here, however, the peak currents [region *c* in Fig. 4(e) and the corresponding current map Fig. 4(c)] are at the higher end of the current range, while region *d* in Fig. 4(e), and the corresponding current map Fig. 4(d) relate to the lower current region. By comparing Fig. 4(b) with the two partial current maps, it becomes evident that each aggregate separates into high-current islands with size down to ~10 nm [Fig. 4(c)], encapsulated by narrow border lines where lower currents are detected [Fig. 4(d)]. These high-current islands correspond most probably to the individual crystallites (or small clusters of them) within an aggregate. Interestingly, it appears that the (relative) current distribution measured on top of the NCs within an aggregate is more homogeneous in the large-NC sample compared to the small-NC sample. In particular, enclosures of lower-current regions, similar to those of the (relatively) higher-current regions described above for the small-NC sample, were rarely observed on the large-NC samples. This issue will be further discussed below.

The dependence of the peak values of the current histograms on the value of the bias at which the measurements were taken is shown in Fig. 5 for both the small- (a) and large- (b) NC samples. For the small-NC sample V_{th} was about −3 V, and the current peak position rises almost linearly with V_B and reaches values of less than 0.1 nA for $V_B=-7.5$ V. For the large-NC sample V_{th} is about −0.5 V, and the peak current rises sharply with V_B and then flattens out at around 20 nA (which is just below the saturation limit of the AFM amplifier) already at V_B of −2 V. We would like to emphasize that Fig. 5 exhibits a very distinctly different current-voltage dependence for the ensembles of the small- and the large-NC-size regimes.

As demonstrated by Fig. 6, the intermediate sample of NCs with $D\sim 10.5$ nm exhibited a more complex behavior than the two current histograms shown above. This complexity is naturally attributed to a combination of the two behaviors that were found for the samples of the small- and large-diameter NCs. At a bias around 3 V the histogram exhibits

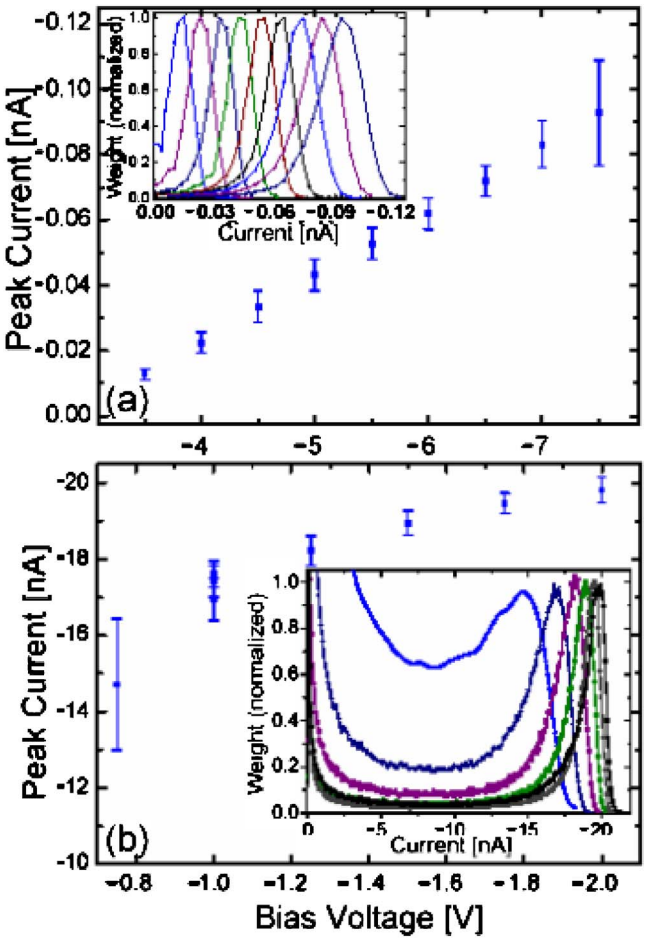

FIG. 5. (Color online) The peak position of the current histograms (shown in the insets) as a function of the bias, for the samples of small (a) and the large (b) NC diameters. Note the large difference in the bias and the current ranges between the two figures.

two peaks, one near the higher end and the other near the lower end of the current range. For $V_B<2.5$ V, only the peak at low currents appears, reminiscent of the one found for small-NC samples, whereas at $V_B>3.5$ V only the peak of the high currents is discernible, as typically observed for the large-NC samples. Figure 6 shows then that this sample manifests a sharp crossover (as a function of bias voltage) of the conductance behavior, from that of the small- to that of the large-NC ensembles. However, the typical currents measured on the intermediate sample are smaller than those observed on the $D>11$ nm NC samples and larger than those measured on the $D<10$ nm NC samples for the same bias values. Note also that at the low bias range ($V_B<2.5$ V) the tail in the current histograms extends to current values that are much higher than those found for the small-NC samples (and are comparable to the peak currents obtained at the same values of the bias for the large-NC samples). This might explain why the macroscopic conductivity of this sample, shown in Fig. 2, was found to be orders of magnitude higher than that of the smaller-NC samples, and yet substantially lower than that of the $D>11$ nm samples. On the other hand this behavior indicates that the conduction is

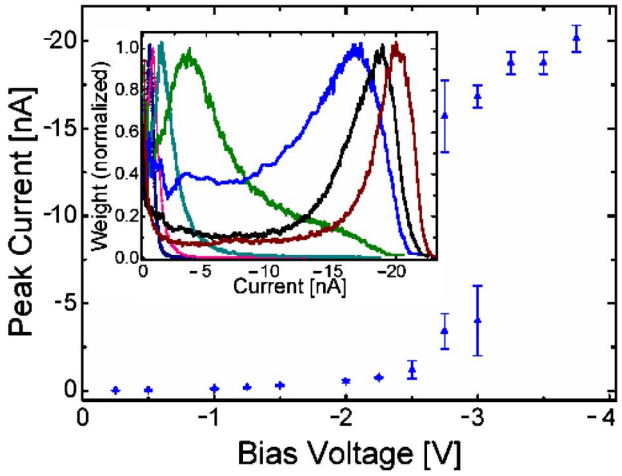

FIG. 6. (Color online) The peak position of the current histograms (shown in the inset) as a function of the bias, for the sample of $D \sim 10.5$ nm. For low bias the peak appears at the lower currents, as in the small-NC samples, but with a long tail extending toward much higher currents. At $V_B = 2.75$ V the high-current tail develops into a second peak, reminiscent of the peaks of the samples of large NCs. As V_B is increased only the second peak is discernible.

not a simple sum of the contributions of NCs belonging to each of the two size regimes (or phases) present in the system, but has to do with a transport mechanism that involves charge transfer between NCs of the different types (see below).

The results presented above were all measured at negative sample bias. A qualitatively similar behavior was observed for positive sample bias, albeit the thresholds for both current detection and the emergence of the peaks in the current histograms were much larger, thus limiting our ability for proper statistical analysis. This asymmetry, which is reflected also in both the STM- and AFM-acquired local current-voltage curves (not shown here), is not directly relevant to the present analysis since it is the same for the large and small NCs, and thus it will be discussed elsewhere.

DISCUSSION

The correlation we found between the topographic and current images suggests that electrical transport takes place through the NCs and not via the grain boundaries or any (possibly different) surrounding phase. This is in contrast to our recent findings[19,20] on polycrystalline CdS films and μc-Si:H, where the current routes were along crystallite or crystallite-aggregate boundaries. While the temperature-dependent macroscopic transport measurements (Fig. 2), as well as the local CAFM data (Figs. 3 and 4), do not enable a precise determination of the conduction mechanism, they suggest some kind of electron tunneling (or hopping) between states localized on neighboring NCs. This suggestion is corroborated by the systematic reduction in conductivity with decreasing NC size that we observed in both local and macroscopic measurements, since the corresponding results are consistent with the effects of quantum confinement and charging. In particular, we note that the same kind of samples studied here exhibit a widening of the optical gap,[3] as to be expected from quantum confinement in the studied range of NC diameters. The remarkable result here is the sharp crossover, as a function of the average NC size in the ensembles, between the two distinct conductivity regimes, observed in both macroscopic (Fig. 2) and local measurements (Fig. 5), which is also manifested in the behavior of the intermediate sample (Fig. 6). Probably the most solid support for the quantum confinement suggestion is derived by considering the 5.6 nm Bohr radius of CdSe. The crossover that we found to take place in the range of average NC diameters of $\sim$10.5 nm appears to signify then the effect of the *degree* of quantum confinement on the transport properties through the NC ensembles. Hence, below the crossover the samples consist mainly of NCs in (although not very deep in) the strong confinement regime (where the NC radius is smaller than the Bohr radius), and above it, where they are predominantly weakly confined. We note in passing that related dimensionality crossover effect was observed in our previous studies of isolated InAs and CdSe nanorods.[11]

The effect of quantum confinement on the NC-ensemble conductivity can be understood as follows. The spacing between the individual NC energy levels increases as the NC size decreases, and, moreover, the sensitivity of the level spacing to the NC diameter becomes more significant in the strong-confinement regime, increasing as the NC size becomes smaller. Let us assume now that charge (electron or hole) transport through the NC ensemble takes place by hopping between (conduction or valence band) states localized on neighboring NCs. The charge carriers will thus flow "more easily" along routes consisting of NCs of similar size so as to minimize the typical energy required for the hopping process. The relatively large NC size distribution, leading to fluctuations of the level spacing from one NC to another, will thus exponentially hinder charge transport through the ensemble. This effect is expected to become more substantial in the small-diameter ($D < 10$ nm, strongly confined) NC samples, where the dependence of the level spectrum on size is much stronger compared to the case in the large-NC ($D > 11$ nm, weakly confined) ensembles. This is also consistent with our observation (see the discussion of Figs. 3 and 4) that the current distribution measured on top of the NC aggregates is much more homogeneous for the large-NC samples, compared to the one measured on the small-NC ensembles: The stronger level structure fluctuation from one NC to another is expected to manifest itself also by significant variations in the conduction routes starting at different NCs on the sample's surface.

The crossover behavior exhibited by the intermediate sample appears to result from a combined contribution of both large and small NCs (recall the relatively wide distribution of the NC sizes), where the former are below the percolation threshold. At low applied bias voltages the conduction takes place through networks comprised solely of the small NCs, where the large NCs are left out due to the large difference between their ground-state levels and those of the smaller NCs. When this barrier is overcome at larger bias values, they join and greatly contribute to the conduction networks.

It should be noted, however, that there may be other factors that can contribute to the above systematic variation of

the conductance properties with NC size. One is the single-NC charging energy which also increases with reduced NC diameter. However, unlike the case of metallic NCs, the charging energies are smaller than those that correspond to quantum confinement. Another factor is the quality of the electrical contact between neighboring NCs, which may improve with increase of the deposition temperature and thus, indirectly, with increase of the NC size. *A priori* one could also attribute the above-described conductivity crossover to a semiconductor-bulk wurtzite–to–zinc blende transition. However, as can be seen in Fig. 2, this will not account for the large decrease in the conductivity and the large increase of the conduction activation energies (which parallels the increase of the optical gap[3]) when the NC size becomes smaller within the range of the mostly wurtzite set of samples ($T_d \leqslant 30$). In addition, we have previously found that in the macroscopic-polycrystalline regime of CdSe the band gap of the bulk zinc-blende phase is larger than that of the bulk wurtzite phase.[22] Considering now the possible effect of the crystal structure, this would imply an increase of the band gap in the wurtzite–to–zinc blende transition, in contrast with our observed[3] decrease of the band gap through the above-described transition region, which we know to be also accompanied by the increase of D in the present NC regime. From the electrical point of view, the larger band gap of the bulk zinc-blende phase should imply also a decrease of the conductivity during the above transition, in contrast with our observations. An interpretation that is consistent with the macroscopic findings of both our previous optical[3] and the present electrical data must attribute the observed changes not to the wurtzite–to–zinc blende transition but to the changes in D. The latter implies a decrease of the band gap (and level spacing within the conduction and valence band states), yielding an increase of the electrical conductivity with increasing D. Consideration of these arguments and the fact that the strongest variations in these properties take place around a D value that is just twice the Bohr radius in CdSe leaves then very little doubt that the observed changes in both the macroscopic and microscopic electrical properties are associated with a quantum confinement effect, in the manner that we suggested above. Further insight into the transport mechanism in the systems we studied can be achieved by performing the same local conductivity measurements but under different conditions, in particular as a function of temperature.

In summary, we have shown, using conductive atomic force microscopy, that in ensembles of CdSe nanocrystallites the current flows through the crystallites themselves and not along their boundaries. The conductivity improves with increasing size of the nanocrystallites, exhibiting a sharp crossoverlike behavior at a diameter range that corresponds to the transition from strong to weak quantum confinement. We explained this behavior by the increased fluctuations in the level structure with the reduction of the average NC size. Support for this picture is gained by our statistical analysis of the CAFM data, including the study of partial current maps.

ACKNOWLEDGMENTS

We thank Inna Popov for the TEM and SEM measurements. This work was supported, in part, by the Israel Science Foundation, the European Union STREP Project SANANO, the DIP program, and the Israel Ministry of Science.

*Corresponding author. Electronic address: balberg@vms.huji.ac.il
†Corresponding author. Electronic address: milode@vms.huji.ac.il

[1] Al. L. Efros and M. Rosen, Annu. Rev. Mater. Sci. **30**, 475 (2000).
[2] V. I. Klimov, *Semiconductor and Metal Nanocrystals, Synthesis and Electronic and Optical Properties* (Marcel Dekker, New York, 2004).
[3] A. Rivera-Marquez, M. Rubin-Falfan, R. Lozada-Morales, O. Portillo-Moreno, O. Zelaya-Angel, J. Luyo-Alvarado, M. Melendez-Lira, and L. Banos, Phys. Status Solidi A **188**, 1059 (2001).
[4] M. V. Artemyev, A. I. Bibik, L. I. Gurinovich, S. V. Gaponenko, and U. Woggon, Phys. Rev. B **60**, 1504 (1999).
[5] M. V. Artemyev, A. I. Bibik, L. I. Gurinovich, S. V. Gaponenko, H. Jaschinski, and U. Woggon, Phys. Status Solidi B **224**, 393 (2001).
[6] D. L. Klein, P. L. McEuen, J. E. Bowen Katari, R. Roth, and A. P. Alivisatos, Appl. Phys. Lett. **68**, 2574 (1996).
[7] O. Millo, D. Katz, Y. W. Cao, and U. Banin, Phys. Rev. Lett. **86**, 5751 (2001).
[8] E. P. A. M. Bakkers and D. Vanmaekelbergh, Phys. Rev. B **62**, R7743 (2000).
[9] T. K. Johal, R. Rinaldi, A. Passaseo, R. Cingolani, A. Vasanelli, R. Ferreira, and G. Bastard, Phys. Rev. B **66**, 075336 (2002).
[10] D. Steiner, D. Katz, O. Millo, A. Aharoni, S. H. Kan, T. Mokari, and U. Banin, Nano Lett. **4**, 1073 (2004).
[11] E. Nahum, E. Ebenstein, A. Aharoni, T. Mokari, U. Banin, N. Shimoni, and O. Millo, Nano Lett. **4**, 103 (2004).
[12] M. Drndic, M. V. Jarosz, N. Y. Morgan, M. A. Kastner, and M. G. Bawendi, J. Appl. Phys. **92**, 7498 (2002).
[13] C. R. Kagan, C. B. Murray, M. Nirmal, and M. G. Bawendi, Phys. Rev. Lett. **76**, 1517 (1996).
[14] D. Yu, Congjun Wang, B. L. Wehrenberg, and P. Guyot-Sionnest, Phys. Rev. Lett. **92**, 216802 (2004).
[15] D. Toker, D. Azulay, N. Shimoni, I. Balberg, and O. Millo, Phys. Rev. B **68**, 041403(R) (2003).
[16] I. Balberg, D. Azulay, D. Toker, and O. Millo, Int. J. Mod. Phys. B **18**, 2091 (2004).
[17] N. Shimoni, D. Azulay, I. Balberg, and O. Millo, Phys. Rev. B **66**, 020102R (2002).
[18] D. Azulay, M. Eylon, O. Eshkenazi, D. Toker, M. Balberg, O. Millo, and I. Balberg, Phys. Rev. Lett. **90**, 236601 (2003).
[19] D. Azulay, O. Millo, S. Silbert, and I. Balberg, Appl. Phys. Lett. **86**, 212102 (2005).
[20] D. Azulay, I. Balberg, V. Chu, J. P. Conde, and O. Millo, Phys. Rev. B **71**, 113304 (2005).
[21] B. Rezek, J. Stuchlík, A. Fejfar, and J. Kočka, J. Appl. Phys. **92**, 587 (2002).
[22] O. Portillo-Moreno, O. Zelaya-Angel, R. Lozada-Morales, M. Rubin-Falfan, and J. A. Rivera-Marquez, Opt. Mater. **18**, 383 (2002).